PHYSICAL REVIEW B **95**, 085106 (2017)

Energy dependence of the electron-boson coupling strength in the electron-doped cuprate superconductor $Pr_{1.85}Ce_{0.15}CuO_{4-\delta}$

M. Beck,[1] M. Klammer,[1] I. Rousseau,[1] M. Obergfell,[1,2] P. Leiderer,[1] M. Helm,[3,4] V. V. Kabanov,[5] I. Diamant,[6] A. Rabinowicz,[6] Y. Dagan,[6] and J. Demsar[1,2,*]

[1]*Department of Physics and Center for Applied Photonics, University of Konstanz, 78457 Konstanz, Germany*

[2]*Institute of Physics, Johannes Gutenberg-University Mainz, 55128 Mainz, Germany*

[3]*Institute of Ion Beam Physics and Materials Research, Helmholtz-Zentrum Dresden-Rossendorf, P.O. Box 510119, 01314 Dresden, Germany*

[4]*Technische Universität Dresden, 01062 Dresden, Germany*

[5]*Jozef Stefan Institute,1000 Ljubljana, Slovenia*

[6]*Raymond and Beverly Sackler School of Physics and Astronomy, Tel Aviv University, 69978 Tel Aviv, Israel*

(Received 20 October 2016; revised manuscript received 18 January 2017; published 3 February 2017)

The quest for a pairing boson in cuprate high-temperature superconductors is one of the outstanding tasks of solid-state physics. Numerous time-resolved studies of pair breaking, related to pairing by time-reversal symmetry, have been performed using femtosecond optical pulses. By considering energy relaxation pathways between charge, spin, and lattice degrees of freedom, evidence for both phonon and antiferromagnetic fluctuation-mediated pairing has been obtained. Here we present a study of the superconducting-state depletion process in an electron-doped cuprate $Pr_{1.85}Ce_{0.15}CuO_{4-\delta}$, where the superconducting gap is smaller than the energy of relevant bosonic excitations. When pumping with above-gap terahertz pulses, we find that the absorbed energy density required to deplete superconductivity, A_{dep}, matches the thermodynamic condensation energy. On the contrary, by near-infrared pumping, A_{dep} is an order of magnitude higher, as in the case of hole-doped, large-gap cuprates. These results imply that only a small subset of bosons, which are generated during the relaxation of optically excited carriers, contributes to pairing. This observation implies that, contrary to the common assumptions, electron-boson coupling in cuprates is strongly energy dependent.

DOI: 10.1103/PhysRevB.95.085106

I. INTRODUCTION

In the last years, numerous femtosecond (fs) real-time studies of carrier dynamics in high-T_c superconductors have been performed, aiming to find the coupling strengths between carriers and other degrees of freedom (high- and low-frequency phonons, spin fluctuations, electronic continuum) [1–14]. In this approach, fs optical pulses are used to excite the electronic system, while the resulting dynamics are probed by measuring the changes in optical constants [1–5,7–12] or the electronic distribution near the Fermi energy [6,13,14]. To connect the measured relaxation time scales to the electron-boson coupling strengths, multitemperature models [15,16] are often used [6,9–11]. These are based on the premise that electron-electron (*e-e*) thermalization is much faster than electron-boson relaxation. While these models are commonly used to extract, e.g., the electron-phonon (e-ph) coupling strengths, numerous inconsistencies have been noted—even for the case of simple metals [17–20].

An alternative time-domain approach, based on the dynamics in the superconducting (SC) state, has been put forward and tested on a conventional BCS superconductor, NbN [21,22]. The approach is based on a well-established fact, that the photoinduced suppression of superconductivity is a nonthermal process, as first demonstrated by Testardi back in 1971 [23]. Following photoexcitation, high-energy carrier relaxation proceeds via carrier-carrier and carrier-boson scattering towards the Fermi energy on a 100-fs timescale. In the presence of a narrow gap in the single-particle density of states, a bottleneck in the relaxation takes place [21,24–26]. Here carriers, accumulated near the gap, form a quasithermal equilibrium with the high-frequency bosons (with $\hbar\omega > 2\Delta$), while the low-frequency ($\hbar\omega < 2\Delta$) modes remain at the base temperature [24,27]. Subsequent recovery of the SC state is governed by the decay of the high-frequency bosons. Interestingly, the boson-bottleneck scenario [21,24–26] seems to be operational also in high-T_c cuprate superconductors. While the existence of gap nodes suggested the absence of a bottleneck and power-law relaxation dynamics, early systematic experimental studies confronted this view [2]. The data suggested that the dynamics is governed by the recombination of antinodal quasiparticles (QPs), rather than relaxation of carriers from antinodal to nodal regions [2]. Indeed, studies of relaxation dynamics in the weak perturbation regime demonstrated excitation-density-dependent relaxation dynamics at low temperatures [5,28], with a diverging relaxation time in the low-perturbation limit [28,29], just as in conventional superconductors [21,22]. The apparent inconsistency of the data with the expected behavior of the *d*-wave gap was theoretically accounted for by Howell, Rosch, and Hirschfeld [30]. They pointed out that the relaxation towards the nodes is blocked by the energy and momentum conservation laws in a *d*-wave BCS superconductor [30]. Indeed, this was demonstrated experimentally by Cortes *et al.* using time-resolved ARPES [31].

Under the assumption that the absorbed optical energy is distributed between QPs and high-frequency ($\hbar\omega > 2\Delta$) bosons on the subpicosecond time scale, and taking into account the nonlinearity of relaxation processes (pairwise recombination of QPs competing with pair breaking by boson reabsorption), the electron-boson coupling strength can be determined by studying the excitation density dependence of

*demsar@uni-mainz.de

the Cooper pair-breaking process [21,22]. While this approach has been successfully applied to conventional superconductors [22,32], the results on cuprate superconductors show that the energy density required to suppress superconductivity exceeds the thermodynamic condensation energy, E_c, by an order of magnitude [7,33–35]. Therefore, the assumption that the absorbed energy is on the ultrafast time scale distributed between quasiparticles and coupled bosonic excitations fails. Considering the possible energy relaxation pathways, the discrepancy observed in hole-doped high-T_c cuprates [7,34,35] has been attributed to the fact that the superconducting gap, 2Δ, lies well within the range of optical phonons [34]. It has been argued that in this case up to 90% of the absorbed energy is via rapid e-ph scattering directly released to $\hbar\omega < 2\Delta$ phonons. These modes (mainly the subgap zone-center optical phonons and zone-edge acoustic phonons) lack the energy to break Cooper pairs. Thus, only ≈10% of the energy is available for condensate depletion [34]. In support of this scenario, it has been demonstrated that in $YBa_2Cu_3O_{7-d}$ the rapid e-ph transfer gives rise to a rapid heating of specific subgap optical phonons on the time scale of ≈100 fs [36]. The above argument can be put to the test by studying cuprate superconductors with a 2Δ far below the energy of optical phonons, as is the case for electron-doped cuprate superconductors [37,38].

Here we present a systematic study of light-induced depletion of superconductivity in an e-doped cuprate superconductor, $Pr_{1.85}Ce_{0.15}CuO_{4-\delta}$ (PCCO), at optimal doping. Indeed, in PCCO $2\Delta \approx 7$ meV [39–42], well below the acoustic phonon cutoff frequency of ≈20 meV [43], as well as the energy of the collective electronic mode of $\approx 11 \pm 2$ meV [44,45]. We used near-infrared ($\lambda = 800$ nm) as well as narrow-band terahertz (THz) ($\nu_{\mathrm{FEL}} = 2.1$ THz, $h\nu_{\mathrm{FEL}} = 8.6$ meV, free space $\lambda = 144$ μm) excitation, while probing the superconducting gap dynamics with THz probe pulses. We expected the absorbed energy density required to deplete the superconductivity, A_{dep}, to be, in the low-temperature limit, the same in the two configurations ($A_{\mathrm{dep}} \approx E_c$). Indeed, this was observed in a conventional superconductor, NbN [22], with similar values of the superconducting gap and the phonon cutoff energy. We demonstrate that this is not the case in PCCO. In fact, similarly to the hole-doped cuprate superconductors, we find for near-infrared (NIR) excitation that $A_{\mathrm{dep}} \gg E_c$. This result implies a strong coupling of high-energy electrons to bosonic excitations, which, however, do not contribute substantially to pairing. In other words, the results suggest that the Eliashberg electron-boson coupling function in cuprates depends strongly on the electron energy, unlike what is commonly considered [16,46].

II. EXPERIMENTAL PROCEDURE

Optimally doped c-axis-oriented PCCO thin films with a thickness $d = 60$ nm were epitaxially grown on $LaSrGaO_4$ (001) (LSGO) substrates using pulsed laser deposition [47]. Inductive measurements of the samples yield a critical temperature $T_c \approx 21$ K.

The broadband linear and time-resolved THz spectroscopy was performed on a setup built around a 250-kHz amplified Ti:sapphire laser system and utilizing a large-area interdigitated photoconductive emitter for the generation of THz pulses [48].

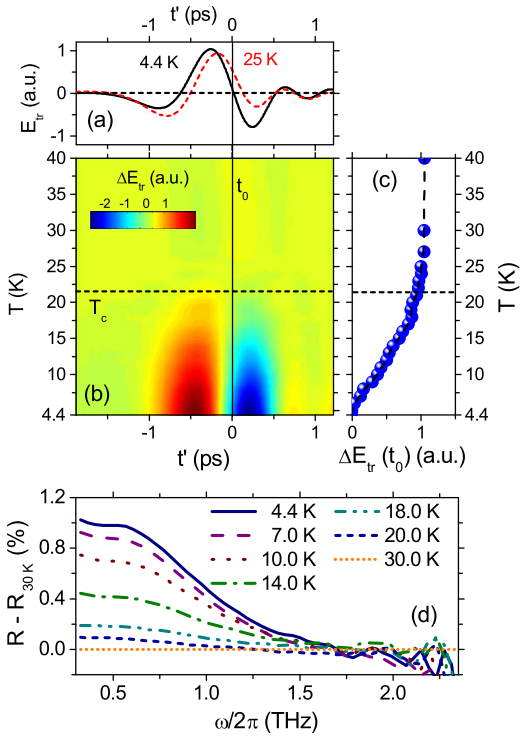

FIG. 1. Temperature dependence of transmitted THz electric-field transients. (a) $E_{\mathrm{tr}}(t')$ in the normal and superconducting states. The pronounced phase shift is characteristic of the inductive response below T_c. (b) $\Delta E_{\mathrm{tr}}(T,t') = E_{\mathrm{tr}}(T,t') - E_{\mathrm{tr}}(25\,\mathrm{K},t')$. (c) Temperature dependence of $\Delta E_{\mathrm{tr}}(T,t_0) = E_{\mathrm{tr}}(T,t_0) - E_{\mathrm{tr}}(4.4\,\mathrm{K},t_0)$. (d) Temperature dependence of the bulk reflectivity extracted from $\sigma(\omega)$.

Equilibrium THz conductivity studies were performed by recording the THz electric fields transmitted through the sample (film on substrate), $E_{\mathrm{tr}}(t')$, and the reference (bare substrate), $E_{\mathrm{re}}(t')$, using the Pockels effect in GaP. The bandwidth was limited by the transverse optical phonon of the LSGO to ≈2.5 THz. The complex optical conductivity $\sigma(\omega) = \sigma_1(\omega) + i\sigma_2(\omega)$ was obtained using the Fresnel equations (see Appendix A and Fig. 5). The normal state $\sigma(\omega)$ can be well approximated by the Drude model. The data at 30 K fit with Drude give the plasma frequency $\nu_p \approx 450$ THz (1.9 eV) and the scattering rate $\tau^{-1} \approx 2.5$ THz (10 meV), in good agreement with optical studies of thick PCCO films [41,42]. To estimate the magnitude of 2Δ, we follow the approach of Ref. [42], where 2Δ is extracted from the reflectivity, by reading out the position in the reflectance spectra, below which the reflectivity starts to rise steeply above its normal-state value. To do so, we use the measured $\sigma(\omega,T)$, calculate the corresponding bulk reflectivity $R(\omega,T)$, and plot $R(\omega,T) - R(\omega,30\,\mathrm{K})$, as shown in Fig. 1(d). It follows that the maximum gap frequency $2\Delta/\hbar \approx 1.7$ THz ($\Delta = 3.5$ meV), in good agreement with other studies on c-axis PCCO films [39,42]. We note that, unlike in the BCS case [22], 2Δ displays only a weak T dependence.

In optical-pump–THz probe experiments, the film is excited by a 50-fs NIR pump pulse centered at 800 nm. The transient spectral conductivity, $\sigma(\omega,t_d)$, is measured as a function of the

time delay t_d between the NIR pump and the THz probe pulse (see Appendix B and Figs. 6 and 7). The initial increase in $\sigma_1(\omega)$ [see Figs. 6(a) and 7(a)] and the concomitant decrease in $\sigma_2(\omega)$ [see Figs. 6(b) and 7(b)] for frequencies below the gap frequency take place on a time scale of several picoseconds (ps). These changes signify the ps depletion of the superconducting state [38]. The recovery of the SC state, marked by the reopening of the gap in $\sigma_1(\omega)$ and the re-establishment of the $\sigma_2(\omega) \propto 1/\omega$ inductive response, proceeds on the much longer time scale of hundreds of ps (see Figs. 6 and 7). For time delays t_d longer than the characteristic e-e and e-ph relaxation times (both of the order of 1 ps) we find that the measured $\sigma(\omega,t_d)$ can be matched to the equilibrium $\sigma(\omega)$ recorded at a specific temperature T^*, i.e., $\sigma(\omega,t_d) \approx \sigma(\omega,T^*)$ (see Fig. 7, Appendix B). This is consistent with the so-called T* model [50], where at nonequilibrium the population of QPs, Cooper pairs, and high-frequency ($\hbar\omega > 2\Delta$) bosons is at quasiequilibrium at temperature T*, which is higher than the base temperature T of $\hbar\omega < 2\Delta$ modes. Given the lack of an analytical model to connect the frequency-dependent optical conductivity in PCCO to Δ, as, e.g., Mattis-Bardeen formulas for an s-wave superconductor in a dirty limit [22,50], we analyze the dynamics in terms of the time evolution of T*.

Narrow-band THz pump-probe experiments were performed at the free electron laser (FEL) facility at the Helmholtz-Zentrum Dresden-Rossendorf. Here, intense narrow-band (spectral width ≈30 GHz, pulse length $\tau_{\rm FEL} \approx$ 18 ps) THz pulses at $\nu_{\rm FEL} = 2.08$ THz, slightly above the low-temperature gap frequency $2\Delta/h \approx 1.7$ THz [39,40], were used as both pump and probe sources using the configuration described in Ref. [49].

III. EXCITATION DEPENDENCE OF SUPERCONDUCTING-STATE DEPLETION

A. Near-infrared excitation

To study the excitation density dependence of the SC-state dynamics over a large range of excitation densities, we recorded the induced changes in the transmitted THz electric field, $\Delta E_{\rm tr}(t',t_d)$, at a fixed $t' = t_0$ as a function of t_d. This approach (see also Refs. [22] and [32]) is justified by the spectrally resolved study presented in Appendix B. As shown in Figs. 1(a)– 1(c) the transmitted electric field $E_{\rm tr}(t')$ depends strongly on the temperature. In particular, for the chosen t_0 (see Fig. 1) $E_{\rm tr}(t_0,T)$ shows a linear T dependence over a large temperature range below T_c.

Figure 2(a) shows the recorded $\Delta E_{\rm tr}(t_0,t_d)$ transients for $T = 4.4$ K and a set of absorbed optical energy densities $A^{\rm NIR}$ (in mJ/cm^3). Here, $A^{\rm NIR}$ is extracted from the incoming laser pulse fluence, F, and the absorption coefficient of PCCO at 800 nm (see Appendix C). The use of an optically thin PCCO film ensures homogeneous excitation throughout the probed volume. It follows from the data that both SC-state depletion and SC-state recovery depend on the excitation density. Similar observations have been made on MgB_2 [32] and NbN [22] and can be well accounted for by the phenomenological Rothwarf-Taylor model [21,24]. In particular, the slow time scale for SC-state depletion (for the lowest excitation densities, several tens of ps!) and its excitation density dependence can be attributed to Cooper pair breaking by $\hbar\omega > 2\Delta$ bosons,

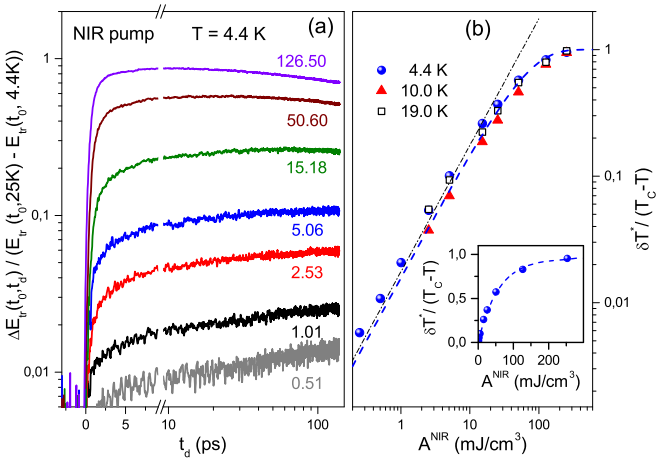

FIG. 2. (a) Transient changes in the transmitted THz electric field, $\Delta E_{\rm tr}(t_0,t_d)$, recorded at 4.4 K for different absorbed energy densities $A^{\rm NIR}$ (in mJ/cm^3). Curves are normalized to the change in $E_{\rm tr}(t_0)$ between 4.4 and 25 K (above T_c). (b) Maximum increase in the effective temperature, δT^*, as a function of $A^{\rm NIR}$ for three base temperatures, normalized to the respective maximum change in T^*, i.e., $T_c - T$. The dashed (blue) line presents the saturation model fit, while the dotted line presents the linear extrapolation. Inset: 4.4 K data on a linear scale.

which are generated during the relaxation of high-energy quasiparticles towards the gap [21,22,32].

Here, we focus on the energetics of the SC-state depletion. We chose $\Delta E_{\rm tr}$ ($t_0,t_d = 30$ ps) to determine the change in effective temperature, δT^*, as a function of the excitation density. The link to T^* is provided by the T dependence of $\Delta E_{\rm tr}(t_0,T)$ at equilibrium, shown in Fig. 1(c), and supported by the spectrally resolved data (see Appendix B). We used a linear interpolation for low excitation densities. The relative change in T^*, $\delta T^*/(T_c - T)$, as a function of $A^{\rm NIR}$ is plotted in Fig. 2(b). For low $A^{\rm NIR}$ the induced changes scale with $A^{\rm NIR}$ yet show the expected saturation at high densities. By applying a simple saturation model fit, where $\frac{\delta T^*}{T_c - T} = 1 - \exp(-A^{\rm NIR}/A^{\rm NIR}_{\rm dep})$, we extract the absorbed energy density required for depleting the SC state, $A^{\rm NIR}_{\rm dep}$. At 4.4 K we find $A^{\rm NIR}_{\rm dep} \approx 60$ mJ/cm^3 ($F^{\rm NIR}_{\rm dep} = 1.6$ μJ/cm^2), comparable to the value obtained on another e-doped cuprate, $Nd_{1.85}Ce_{0.15}CuO_{4+\delta}$ [51]. This energy is about six times the superconducting-state condensation energy of PCCO, $E_c \simeq$ 10 mJ/cm^3 [52], following the trend of hole-doped cuprates, where $A^{\rm NIR}_{\rm dep} \gg E_c$ [7,34,35]. We note that $A^{\rm NIR}_{\rm dep}$ is, at the same time, substantially lower than the energy needed to thermally suppress superconductivity, $E_{\rm th}$. The latter is given by $E_{\rm th} = \int_{4.4\,\rm K}^{21\,\rm K} C_p(T)dT \simeq 250$ mJ cm^{-3}, where $C_p(T)$ is the total specific heat [52]. This implies that also in PCCO the light-induced depletion of superconductivity is nonthermal, with low-energy bosons still being at the base temperature. Indeed, as shown in Appendix D, the energy initially released to low-energy acoustic phonons is negligible.

B. Above-gap THz excitation

We studied the SC-state depletion in PCCO using intense narrow-band THz pulses in a single-color pump-probe scheme

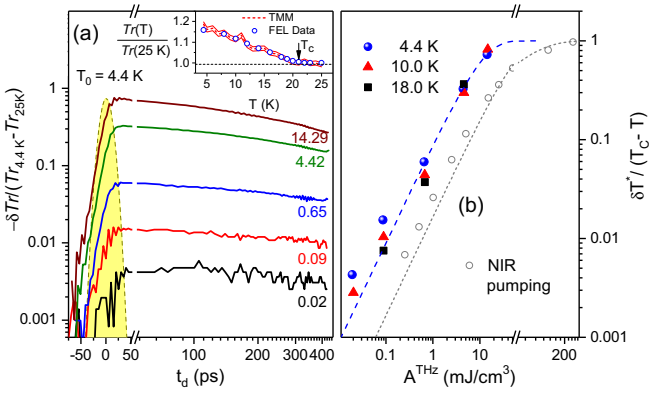

FIG. 3. (a) Changes in the THz transmission intensity δTr after photoexcitation with intense THz pulses at $T = 4.4$ K [absorbed energy densities A^{THz} (in mJ/cm^3) are listed]. The shaded area presents the cross-correlation of narrow-band THz pulses. Inset: T dependence of equilibrium Tr. The measured transmission in the FEL setup matches well the transfer-matrix method (TMM) calculation based on the measured $\sigma(\omega)$. (b) Change in the effective temperature δT^* as a function of A^{THz} for three base temperatures. The dashed blue line is the fit with the simple saturation model. Open gray circles and the dotted gray line present the data obtained by NIR pumping for comparison.

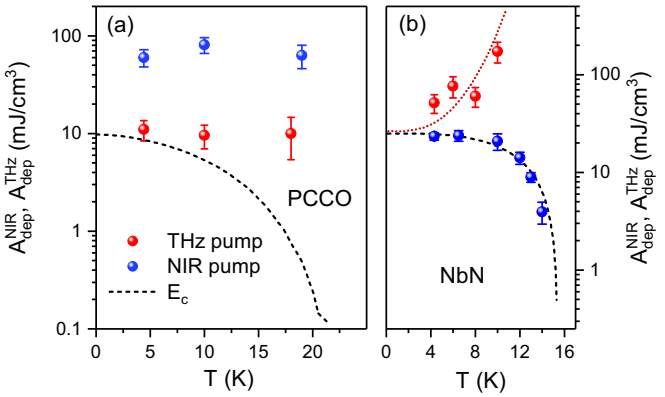

FIG. 4. (a) Absorbed optical energy density required for superconducting-state depletion in PCCO during pumping with NIR (1.5-eV) and THz (8.6-meV) pulses. The dashed line is the superconducting condensation energy from Ref. [52]. (b) For comparison, the corresponding data on NbN taken from Ref. [49]. The red dotted line is a guide to the eye.

[49]. The temperature dependence of the transmission intensity (Tr) at equilibrium is shown in the inset to Fig. 3(a). The measurements agree with the transfer-matrix method calculation based on the optical conductivity data obtained by broadband THz spectroscopy (Appendix A). With THz excitation the superconductivity is perturbed directly, with QPs having close to 0 excess energy. Still, due to quasiparticle recombination via emission of $\hbar\omega > 2\Delta$ bosons and boson reabsorption, quasiequilibrium between the condensate, QPs, and $\hbar\omega > 2\Delta$ bosons (described by T^*) should be reached within tens of ps, similar to the case of NIR pumping.

Figure 3(a) presents the time evolution of the normalized pump-induced changes in THz transmission at 2.1 THz (δTr) recorded for several A^{THz} values. The shaded area corresponds to the intensity cross-correlation of narrow-band THz pulses. Unlike in the NIR pump experiments, no delayed SC-state depletion dynamics is observed to take place beyond the THz pump pulse duration, despite the fact that the lowest excitation densities in the THz pump experiments were an order of magnitude lower than in the NIR pump study. This clearly demonstrates different excitation mechanisms in the two configurations [21]. While with pumping with THz photons with $\nu_{\mathrm{FEL}} > 2\Delta/\hbar$, Cooper pairs are broken directly, with NIR pumping, Cooper pairs are broken mainly by $\hbar\omega > 2\Delta$ bosons generated during the cascade of high-energy QPs towards the gap edge.

Assuming the T^* approximation as for NIR pumping, we convert the maximum induced changes in Tr into changes in T^*, using the calibration curve in the inset in Fig. 3(a). Figure 3(b) summarizes the results for three base temperatures, indicating similar values of $A^{\mathrm{THz}}_{\mathrm{dep}}$.

Contrary to $A^{\mathrm{NIR}}_{\mathrm{dep}}$, $A^{\mathrm{THz}}_{\mathrm{dep}}$ (4.4 K) ≈ 11 mJ/cm^3 is within error bars identical to E_c. This implies that almost all of the deposited energy is directly used for condensate depletion and only a miniscule amount of energy is transferred into the bosonic system. Since the recovery dynamics is identical for the two excitation processes and can be attributed to the boson-bottleneck scenario [21,24], some energy has to be transferred to the $\hbar\omega > 2\Delta$ bosonic modes. As pointed out above, the excited state can be described by the effective temperature T^*. Here the quasiparticle density, $n_{\mathrm{qp}} \propto \exp(-\Delta/k_B T^*)$, and the density of $\hbar\omega > 2\Delta$ bosons, $n_b \propto \exp(-2\Delta/k_B T^*)$, follow the detailed balance equation, $n_b \propto n_{\mathrm{qp}}^2$ [21,24,32]. It follows [22] that for moderate excitation densities, where $\Delta > k_B T^*$, the vast majority of the energy is stored in the electronic subsystem, consistent with the observation that at low temperatures $A^{\mathrm{THz}}_{\mathrm{dep}} \approx E_c$.

Figure 4 summarizes the dependence of A_{dep} on the pump photon energy and temperature. The observation that the low-T value of $A^{\mathrm{THz}}_{\mathrm{dep}}$ matches E_c is consistent with expectations. Far more surprising is the result of the NIR pumping experiment in PCCO, where $A^{\mathrm{NIR}}_{\mathrm{dep}} \gg E_c$.

IV. DISCUSSION AND CONCLUSIONS

In hole-doped cuprates, considering the fast condensate depletion times and specific heats of different bosonic subsystems (phonons, spin fluctuations), the observation that $A^{\mathrm{NIR}}_{\mathrm{dep}} \gg E_c$ was attributed to the dominant e-ph (pairing) interaction [7]. Considering the energy and momentum conservation during relaxation [53], the rapid e-ph relaxation process generates predominantly optical phonons near $q = 0$ and high-energy (zone-edge) acoustic phonons [34] (see also Appendix D). Here, $\hbar\omega > 2\Delta$ phonons couple to the condensate via pair breaking (and repairing), giving rise to the depletion of superconductivity. On the other hand, a large amount of the absorbed energy is rapidly transferred to optical and zone-edge acoustic phonons with $\hbar\omega < 2\Delta$ [34,35]. These lack the energy for breaking-up of Cooper pairs, thus acting as an effective heat sink.

For superconductors with 2Δ below the acoustic phonon cutoff, however, $A^{\mathrm{NIR}}_{\mathrm{dep}} \approx E_c$ is expected. Indeed, this has been demonstrated in NbN [22] and ferropnictides [35].

Since in PCCO $2\Delta \approx 7$ meV is far below the acoustic phonon cutoff energy of ≈20 meV [43], as well as the energy of the collective electronic mode of $\approx 11 \pm 2$ meV [44,45], the interpretation put forward for hole-doped cuprates [34,35] is challenged. The result that $A_{\rm dep}^{\rm NIR} \gg E_c$ in small-gap electron-doped cuprates implies a rapid *electron-boson* energy transfer following NIR pumping, yet *only selected bosonic modes couple to the condensate by Cooper pair breaking*.

The observation that in the low-T limit $A_{\rm dep}^{\rm NIR} \gg A_{\rm dep}^{\rm THz} \approx E_c$ in PCCO implies, quite generally, that the Eliashberg electron-boson coupling function strongly depends on the electron energy. The electron-boson spectral function $\alpha^2F(\varepsilon,\varepsilon',\Omega)$, where ε and ε' are the electronic and Ω the bosonic energy, is commonly approximated by $\alpha^2F(\varepsilon_F,\varepsilon_F,\Omega) = \alpha^2F(\Omega)$, since it is customary to assume that its variation on ε and ε' on an energy scale smaller than the electronic bandwidth can be neglected [46]. In other words, it is expected that the electron-boson coupling strength is roughly independent of the electron energy (within the electronic bandwidth). In this case, the dominant electron-boson interaction responsible for relaxation of hot carriers towards the gap edge should also be the dominant electron-boson interaction responsible for pairing (and pair breaking). Our result, that with NIR pumping a large part of the energy is rapidly transferred to bosonic excitations, which do not couple to the condensate, suggests the failure of the above assumption in e-doped PCCO. For electron energies of the order of 1 eV the e-e scattering process dominates the electron-boson scattering [54], thereby substantially reducing the average electron excess energy on the time scale of a few femtoseconds [54]. Hot carrier relaxation becomes dominated by electron-boson scattering when hot carriers reach an energy range of the order of $\varepsilon \approx \sqrt{\omega_D E_F} \approx 300$ meV (assuming the phonon cutoff energy $\omega_D \approx 80$ meV and the Fermi energy $E_F \approx 1$ eV). This suggests that α^2F changes dramatically on an energy scale of the order of 100 meV, i.e., somewhere between ≈300 and 10 meV.

We should also mention that no significant variation of $A_{\rm dep}$ with the temperature is observed in either of the two configurations. This is not surprising for NIR pumping, where $A_{\rm dep}^{\rm NIR} \gg E_c$ and only ≈15% of the absorbed energy is used for condensate depletion. The fact that a similar situation is observed with THz pumping is puzzling. We speculate that this may be linked to the effects of enhancement of SC due to nonequilibrium electron distribution, which was observed recently in NbN for temperatures close to T_c [49].

By speculating a similar origin behind the observation that $A_{\rm dep}^{\rm NIR} \gg E_c$ in hole-doped cuprates [7,34–36], one can argue that a strong dependence of α^2F on the electron energy is a common property of high-temperature superconducting cuprates. Considering the competing scenarios of superconductivity being mediated by phonons versus magnetic excitations, the result suggests that high-energy electrons strongly couple to either phonons or magnetic modes, while the situation is reversed for low-energy electrons. As mentioned above, a recent optical pump-broadband THz probe study [36] on YBCO demonstrated directly that NIR pumping results in (over)heating of selected optical phonons on the 100-fs time scale [36], implying a very strong electron-phonon coupling (at least for hot carriers). Yet, as in PCCO, $A_{\rm dep}^{\rm NIR} \approx 5 - 10E_c$ in YBCO [35], implying that these modes weakly couple to the condensate. Thus, we may conclude that pairing in cuprates is mediated by magnetic excitations. Alternatively, we could assume that high-energy electrons emit magnetic excitation on the fs time scale, as recently suggested [55]. If this is the case, these nonequilibrium magnetic excitations are almost uncoupled from the condensate and therefore do not act as pair breakers.

We note that the proposed scenario is based on the very simple observation that the excitations created by high-energy electrons poorly couple to the condensate. Therefore the pair-breaking times due to this coupling are longer than the anharmonic decay of these excitations. As a result, the Rothwarf-Taylor bottleneck [21] is not operational for these excitations.

For further insight, direct access to the time evolution of the population of bosonic excitations in an energy- and momentum-resolved fashion is required. Here, further development of scattering techniques like femtosecond x-ray [56] and electron [57] diffuse scattering and even spectroscopy [58] is expected to play a crucial role.

ACKNOWLEDGMENTS

We thank P. Michel and the FELBE team for their dedicated support. This work was supported by the German Research Foundation (Deutsche Forschungsgemeinschaft) through Transregional Collaborative Research Center 173 "Spin + X," Project No. A05, German-Israeli DIP Project No. 563363, and the Kurt Lion Foundation. Y.D. acknowledges support from the Israel Science Foundation under Grant No. 569/13.

APPENDIX A: TEMPERATURE DEPENDENCE OF COMPLEX OPTICAL CONDUCTIVITY

Figure 5 presents the temperature dependence of the equilibrium THz conductivity of an electron-doped cuprate superconductor, $Pr_{1.85}Ce_{0.15}CuO_{4-\delta}$ (PCCO), at optimal doping. The results are similar to published data obtained by infrared spectroscopy [41,42].

In the absence of a generally accepted model for fitting the optical conductivity of a d-wave superconductor to extract the gap magnitude, we follow the approach of Homes *et al.* [42]. Here 2Δ was extracted from the reflectivity data by reading out the position in the reflectance spectra below which the reflectivity starts to rise steeply above its normal-state value. To do so, we used the measured $\sigma(\omega,T)$ and calculated the corresponding bulk reflectivity $R(\omega,T)$, which is shown in Fig. 5(c). It follows that the maximum gap frequency $2\Delta/\hbar \approx 1.7$ THz ($\Delta = 3.5$ meV), in good agreement with other measurements on c-axis films [39,42].

APPENDIX B: PHOTOINDUCED DYNAMICS OF COMPLEX OPTICAL CONDUCTIVITY

Figure 6 presents the time evolution of the complex optical conductivity following photoexcitation of PCCO at 4.4 K. The change in the THz conductivity upon optical pumping at 4.4 K is shown in Figs. 6(a) and 6(b). Here the conductivity change is plotted as a function of the time delay t_d between

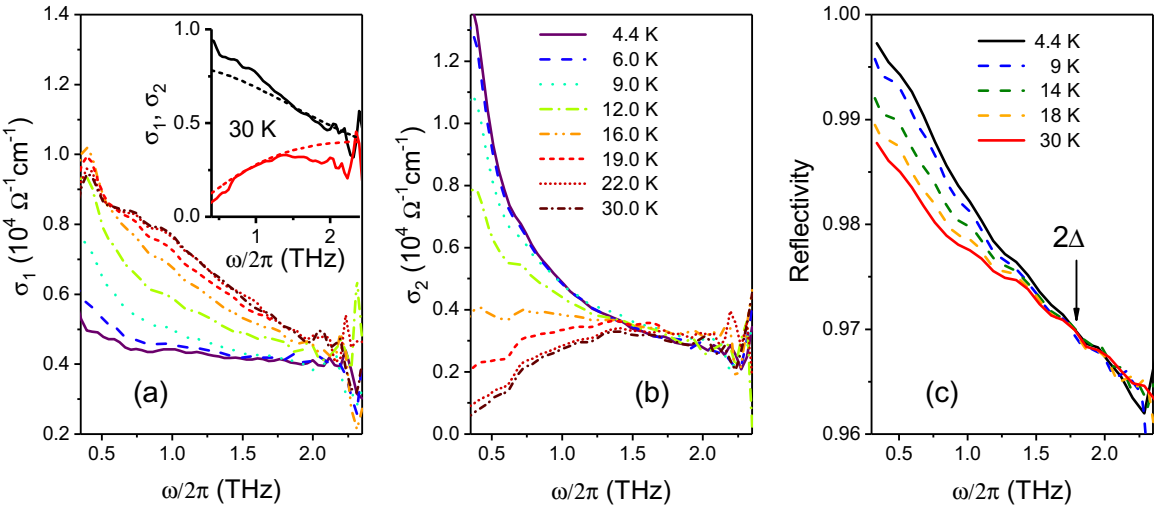

FIG. 5. Temperature dependence of (a) the real and (b) the imaginary part of the optical conductivity $\sigma(\omega)$. Inset in (a): $\sigma_1(\omega)$ (solid black line) and $\sigma_2(\omega)$ (solid red line) at 30 K, together with the corresponding fit with the Drude model (dashed lines). Opening of the superconducting gap below $T_c = 22$ K gives rise to a reduction in $\sigma_1(\omega)$, while $\sigma_2(\omega)$ displays a $1/\omega$ inductive response. (c) The corresponding bulk reflectivities under normal incidence obtained from measured $\sigma(\omega)$.

the optical pump and the THz probe pulse. For comparison we plot changes in conductivities induced by heating the sample [Figs. 6(c) and 6(d)]. Clear similarities are seen when comparing Figs. 6(a) and 6(c) and Figs. 6(b) and 6(d). The suppression of superconductivty takes place on a ps time scale, as shown in the color plots. Recovery of the superconducting state proceeds on the 100-ps time scale.

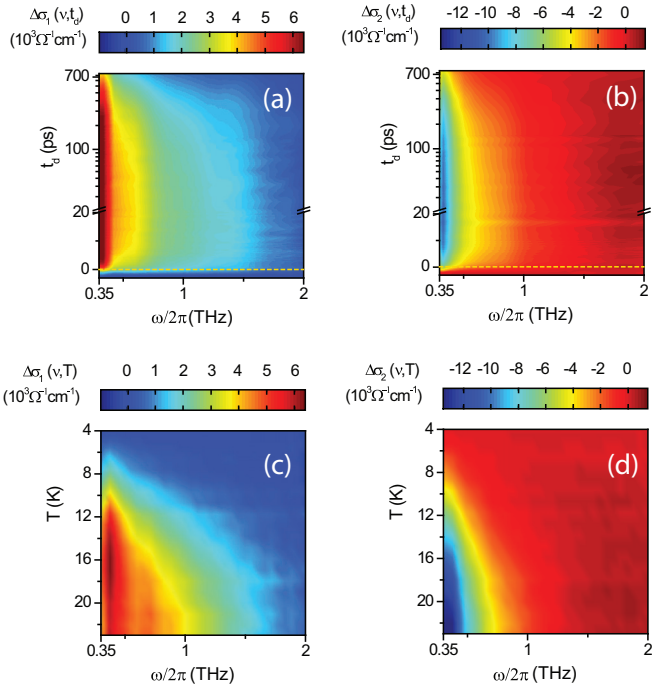

FIG. 6. Change in (a) the real and (b) the imaginary conductivity $\Delta\sigma(\omega,t_d)$ following optical excitation (indicated by the dashed orange line at $t_d = 0$) at $T = 4.4$ K. The difference between the excited and the unexcited conductivities is plotted. The excitation density corresponds to the absorbed energy density of $\sim 50\,\mathrm{mJ/cm^3}$. For comparison, the temperature dependence of (c) the real and (d) the imaginary parts of the optical conductivity is shown. Spectra show the change in conductivity given by $\Delta\sigma_i = \sigma_i(T) - \sigma_i(4.4\ \mathrm{K})$ with $(i = 1, 2)$. The color map is identical for all panels, for direct comparison.

To depict a more quantitative picture of the observed THz conductivity dynamics, the spectral conductivity data for selected time delay values t_d are directly compared to the measured temperature-dependent data. Mathematically, the determination of T^* equals solving the variational problem $\min_{T^*}\{\|\sigma(\omega,t_d) - \sigma(\omega,T^*)\|\}$. Thus, T^* marks the temperature where the nonequilibrium conductivity best matches the conductivity in equilibrium.

Figure 7 shows the result of this procedure for a set of time delays. For both σ_1 and σ_2 at nonequilibrium, we find a good agreement with the equilibrium conductivity at a certain

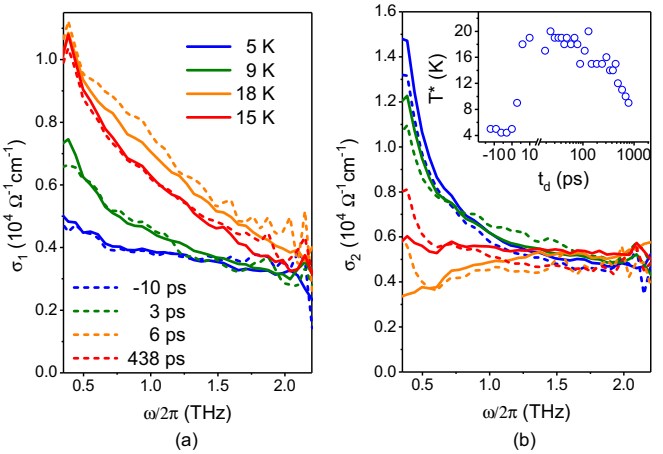

FIG. 7. Comparison of the spectral conductivity data for selected time delay values, t_d, with the measured temperature-dependent data at equilibrium. (a) Values of t_d and the corresponding T^* for the plotted data are listed. Inset in (b): Evolution of the extracted T^* as a function of t_d.

temperature. The inset in Fig. 7(b) shows the resulting $T^*(t_d)$ obtained by solving the variational problem for every measured t_d. T^* increases quickly to values close to T_c, on the time scale of a few ps. Thus, after strong optical excitation (the excitation density used here is $A = 50$ mJ cm^{-3}), a rapid suppression of superconductivity is observed. The energy needed to heat up the photoexcited sample volume from the 4.4 K base temperature to close to T_c is $E_{\rm th} = \int_{4.4\,\rm K}^{21\,\rm K} C_p(T)dT \approx 250$ mJ cm^{-3}, with C_p being the experimentally measured total specific heat [52]. Thus, the extracted T^* represents the effective temperature of the electronic system thermalized with high-frequency ($\omega > 2\Delta$) bosons, while the low-frequency ($\omega < 2\Delta$) modes are still at the base temperature (see also Appendix D).

APPENDIX C: DETERMINATION OF THE ABSORBED ENERGY DENSITY BY NIR

The optical penetration depth $l_{\rm opt}$ is given by $l_{\rm opt} = \frac{\lambda_0}{4\pi k}$, where k is the imaginary part of the refractive index, which can be calculated from the complex optical conductivity, $\sigma(\omega)$. The complex optical conductivity at 1.55 eV (800 nm), obtained via Kramers-Kronig analysis of optical reflectivity [42], is $\sigma(1.5\ \text{eV}) = 230 + i250\ \Omega^{-1}\,\text{cm}^{-1}$. The corresponding optical penetration depth is $l_{\rm opt} \approx 180$ nm. We have also measured the reflectivity (R) and transmission (T) at near-normal incidence through our 60-nm PCCO film on a 0.5-mm LSGO substrate. The experimental values, $T \approx 60\%$ and $R \approx 16\%$, are in good agreement (within 2%) with the transfer-matrix calculation using the above values of optical constants, and $n_{\rm LSGO} \approx 2$. Thus, $\approx$22% of the incoming intensity is absorbed in the film, and we have a nearly homogeneous excitation level along the film thickness. The latter is important for performing quantitative analysis.

The on-sample spot size diameter of the NIR pump beam was 1.8 mm (FWHM). For the THz probe pulse the spot size naturally depends on the frequency. We have determined the spot size using the knife-edge method. Here the FWHM ranges from 0.9 mm (at 0.4 THz), to 0.45 mm (at 1 THz), to 0.25 mm (at 3 THz). This further implies a nearly homogeneous excitation level throughout the probed volume.

Since the excitation density is extremely homogeneous, no complicated formulas to determine the depth or radial-dependent optical deposited energy density are required. The absorbed energy density is simply given by $A = F\alpha/d$, where F is the fluence at the sample position, $\alpha = 0.22$, and $d = 60$ nm is the film thickness.

APPENDIX D: PHONON GENERATION BY HOT ELECTRONS

According to the linearized kinetic equations, given by Eqs. 18 and 19 in Ref. [59], the generation of phonons by hot electrons is determined by the term F_3. Taking into account that the energy of hot electrons, ξ, is high compared to the Debye energy, $\hbar\omega_D$, we may write the following equation for the nonequilibrium distribution function of phonons:

$$\delta f(\omega) \propto \alpha^2 F(\omega)/\omega^2. \tag{D1}$$

In the clean limit $\omega_D\tau \gg 1$ (where τ is the electron relaxation time), with $\alpha^2 F(\omega) \propto \omega^2$, the generated nonequilibrium phonons have a distribution function which is independent of the energy. In the opposite case of a dirty metal, $\omega_D\tau \ll 1$, where the Eliashberg function is $\alpha^2 F(\omega) \propto \omega$, the nonequilibrium distribution function of phonons is $\delta f(\omega) \propto 1/\omega$. Thus, we can evaluate the energy accumulated in low-frequency (acoustic) phonons during hot-electron relaxation:

$$\Delta E = \int_0^{2\Delta} \delta f(\omega) D(\omega) \omega d\omega. \tag{D2}$$

Here $D(\omega) \propto \omega^2$ is the phonon density of states and Δ is the superconducting gap. In the clean limit ($\omega_D\tau \gg 1$), as is the case in PCCO, the energy fraction accumulated in low-frequency phonons after the initial relaxation is small as $(2\Delta/\omega_D)^4$. Taking the value of $2\Delta = 7$ meV [39,40] and an acoustic phonon cutoff frequency of $\approx$20 meV [43] the energy fraction accumulated in low-frequency phonons amounts to a few percent.

[1] J. Demsar, B. Podobnik, V. V. Kabanov, Th. Wolf, and D. Mihailovic, Phys. Rev. Lett. **82**, 4918 (1999).

[2] V. V. Kabanov, J. Demsar, B. Podobnik, and D. Mihailovic, Phys. Rev. B **59**, 1497 (1999).

[3] R. A. Kaindl, M. Woerner, T. Elsaesser, D. C. Smith, J. F. Ryan, G. A. Farnan, M. P. McCurry, and D. G. Walmsley, Science **287**, 470 (2000).

[4] R. D. Averitt, G. Rodriguez, A. I. Lobad, J. L. W. Siders, S. A. Trugman, and A. J. Taylor, Phys. Rev. B **63**, 140502 (2001).

[5] R. A. Kaindl, M. A. Carnahan, D. S. Chemla, S. Oh, and J. N. Eckstein, Phys. Rev. B **72**, 060510(R) (2005).

[6] L. Perfetti, P. A. Loukakos, M. Lisowski, U. Bovensiepen, H. Eisaki, and M. Wolf, Phys. Rev. Lett. **99**, 197001 (2007).

[7] P. Kusar, V. V. Kabanov, S. Sugai, J. Demsar, T. Mertelj, and D. Mihailovic, Phys. Rev. Lett. **101**, 227001 (2008).

[8] C. Gadermaier, A. S. Alexandrov, V. V. Kabanov, P. Kusar, T. Mertelj, X. Yao, C. Manzoni, D. Brida, G. Cerullo, and D. Mihailovic, Phys. Rev. Lett. **105**, 257001 (2010).

[9] S. Dal Conte, C. Giannetti, G. Coslovich, F. Cilento, D. Bossini, T. Abebaw, F. Banfi, G. Ferrini, H. Eisaki, M. Greven, A. Damascelli, D. van der Marel, and F. Parmigiani, Science **335**, 1600 (2012).

[10] B. Mansart, D. Boschetto, A. Savoia, F. Rullier-Albenque, F. Bouquet, E. Papalazarou, A. Forget, D. Colson, A. Rousse, and M. Marsi, Phys. Rev. B **82**, 024513 (2010).

[11] E. E. M. Chia, D. Springer, S. K. Nair, X. Q. Zou, S. A. Cheong, C. Panagopoulos, T. Tamegai, H. Eisaki, S. Ishida, S. Uchida, A. J. Taylor, and J.-X. Zhu, New J. Phys. **15**, 103027 (2013).

[12] L. Stojchevska, P. Kusar, T. Mertelj, V. V. Kabanov, X. Lin, G. H. Cao, Z. A. Xu, and D. Mihailovic, Phys. Rev. B **82**, 012505 (2010).

[13] L. Rettig, R. Cortes, S. Thirupathaiah, P. Gegenwart, H. S. Jeevan, M. Wolf, J. Fink, and U. Bovensiepen, Phys. Rev. Lett. **108**, 097002 (2012).

[14] C. L. Smallwood, J. P. Hinton, C. Jozwiak, W. Zhang, J. D. Koralek, H. Eisaki, D.-H. Lee, J. Orenstein, and A. Lanzara, Science **336**, 1137 (2012).

[15] M. I. Kaganov, I. M. Lifshitz, and L. V. Tantarov, Zh. Eksp. Teor. Fiz. **31**, 232 (1956) [Sov. Phys. JETP **4**, 173 (1957)].

[16] P. B. Allen, Phys. Rev. Lett. **59**, 1460 (1987).

[17] W. S. Fann, R. Storz, H. W. K. Tom, and J. Bokor, Phys. Rev. Lett. **68**, 2834 (1992); Phys. Rev. B **46**, 13592 (1992).

[18] R. H. M. Groeneveld, R. Sprik, and A. Lagendijk, Phys. Rev. B **51**, 11433 (1995).

[19] V. V. Kabanov and A. S. Alexandrov, Phys. Rev. B **78**, 174514 (2008).

[20] J. Demsar and T. Dekorsy, in *Optical Techniques for Solid-State Materials Characterization*, edited by R. P. Prasankumar and A. J. Taylor (Francis & Taylor, New York, 2011).

[21] V. V. Kabanov, J. Demsar, and D. Mihailovic, Phys. Rev. Lett. **95**, 147002 (2005).

[22] M. Beck, M. Klammer, S. Lang, P. Leiderer, V. V. Kabanov, G. N. Gol'tsman, and J. Demsar, Phys. Rev. Lett. **107**, 177007 (2011).

[23] L. R. Testardi, Phys. Rev. B **4**, 2189 (1971).

[24] A. Rothwarth and B. N. Taylor, Phys. Rev. Lett. **19**, 27 (1967).

[25] J. Demsar, V. K. Thorsmolle, J. L. Sarrao, and A. J. Taylor, Phys. Rev. Lett. **96**, 037401 (2006).

[26] J. Demsar, J. L. Sarrao, and A. J. Taylor, J. Phys. Condens. Matter **18**, R281 (2006).

[27] A. G. Aronov and B. Z. Spivak, J. Low Temp. Phys. **29**, 149 (1977).

[28] N. Gedik, P. Blake, R. C. Spitzer, J. Orenstein, R. Liang, D. A. Bonn, and W. N. Hardy, Phys. Rev. B **70**, 014504 (2004).

[29] J. Demsar, R. Hudej, J. Karpinski, V. V. Kabanov, and D. Mihailovic, Phys. Rev. B **63**, 054519 (2001).

[30] P. C. Howell, A. Rosch, and P. J. Hirschfeld, Phys. Rev. Lett. **92**, 037003 (2004).

[31] R. Cortes, L. Rettig, Y. Yoshida, H. Eisaki, M. Wolf, and U. Bovensiepen, Phys. Rev. Lett. **107**, 097002 (2011).

[32] J. Demsar, R. D. Averitt, A. J. Taylor, V. V. Kabanov, W. N. Kang, H. J. Kim, E. M. Choi, and S. I. Lee, Phys. Rev. Lett. **91**, 267002 (2003).

[33] C. Giannetti, G. Zgrablic, C. Consani, A. Crepaldi, D. Nardi, G. Ferrini, G. Dhalenne, A. Revcolevschi, and F. Parmigiani, Phys. Rev. B **80**, 235129 (2009).

[34] M. Beyer, D. Städter, M. Beck, H. Schäfer, V. V. Kabanov, G. Logvenov, I. Bozovic, G. Koren, and J. Demsar, Phys. Rev. B **83**, 214515 (2011).

[35] L. Stojchevska, P. Kusar, T. Mertelj, V. V. Kabanov, Y. Toda, X. Yao, and D. Mihailovic, Phys. Rev. B **84**, 180507(R) (2011).

[36] A. Pashkin, M. Porer, M. Beyer, K. W. Kim, A. Dubroka, C. Bernhard, X. Yao, Y. Dagan, R. Hackl, A. Erb, J. Demsar, R. Huber, and A. Leitenstorfer, Phys. Rev. Lett. **105**, 067001 (2010).

[37] N. P. Armitage, P. Fournier, and R. L. Greene, Rev. Mod. Phys. **82**, 2421 (2010).

[38] D. N. Basov and T. Timusk, Rev. Mod. Phys. **77**, 721 (2005).

[39] Y. Dagan, R. Beck, and R. L. Greene, Phys. Rev. Lett. **99**, 147004 (2007).

[40] I. Diamant, R. L. Greene, and Y. Dagan, Phys. Rev. B **80**, 012508 (2009).

[41] A. Zimmers, R. P. S. M. Lobo, N. Bontemps, C. C. Homes, M. C. Barr, Y. Dagan, and R. L. Greene, Phys. Rev. B **70**, 132502 (2004).

[42] C. C. Homes, R. P. S. M. Lobo, P. Fournier, A. Zimmers, and R. L. Greene, Phys. Rev. B **74**, 214515 (2006).

[43] I. W. Sumarlin, J. W. Lynn, D. A. Neumann, J. J. Rush, J. L. Peng, Z. Y. Li, and S. J. Hagen, Physica C **185-189**, 2571 (1991).

[44] S. D. Wilson, P. Dai, S. Li, S. Chi, H. J. Kang, and J. W. Lynn, Nature **442**, 59 (2006).

[45] F. C. Niestemski, S. Kunwar, S. Zhou, S. Li, H. Ding, Z. Wang, P. Dai, and V. Madhavan, Nature **450**, 1058 (2007).

[46] P. B. Allen and B. Mitrovic, Solid State Phys. **37**, 1 (1982).

[47] E. Maiser, P. Fournier, J. L. Peng, F. M. Araujo-Moreira, T. Venkatesan, R. L. Greene, and G. Czjzek, Physica C **297**, 15 (1998).

[48] M. Beck, H. Schäfer, G. Klatt, J. Demsar, S. Winnerl, M. Helm, and T. Dekorsy, Opt. Express **18**, 9251 (2010).

[49] M. Beck, I. Rousseau, M. Klammer, P. Leiderer, M. Mittendorff, S. Winnerl, M. Helm, G. N. Gol'tsman, and J. Demsar, Phys. Rev. Lett. **110**, 267003 (2013).

[50] M. Tinkham, *Introduction to Superconductivity* (McGraw–Hill, New York, 1996).

[51] J. P. Hinton, J. D. Koralek, G. Yu, E. M. Motoyama, Y. M. Lu, A. Vishwanath, M. Greven, and J. Orenstein, Phys. Rev. Lett. **110**, 217002 (2013).

[52] H. Balci and R. L. Greene, Phys. Rev. B **70**, 140508(R) (2004).

[53] In PCCO, as in cuprates in general, $\Omega\tau \gg 1$ (Ω is the phonon cutoff angular frequency and τ the momentum scattering time), thus the energy and momentum conservation is fulfilled.

[54] W. Nessler, S. Ogawa, H. Nagano, H. Petek, J. Shimoyama, Y. Nakayama, and K. Kishio, Phys. Rev. Lett. **81**, 4480 (1998).

[55] S. Dal Conte, L. Vidmar, D. Golež, M. Mierzejewski, G. Soavi, S. Peli, F. Banfi, G. Ferrini, R. Comin, B. M. Ludbrook, L. Chauviere, N. D. Zhigadlo, H. Eisaki, M. Greven, S. Lupi, A. Damascelli, D. Brida, M. Capone, J. Bonča, G. Cerullo, and C. Giannetti, Nature Phys. **11**, 421 (2015).

[56] M. Trigo, J. Chen, V. H. Vishwanath, Y. M. Sheu, T. Graber, R. Henning, and D. A. Reis, Phys. Rev. B **82**, 235205 (2010).

[57] T. Chase, M. Trigo, A. H. Reid, R. Li, T. Vecchione, X. Shen, S. Weathersby, R. Coffee, N. Hartmann, D. A. Reis, X. J. Wang, and H. A. Dürr, Appl. Phys. Lett. **108**, 041909 (2016).

[58] F. Carbone, O.-H. Kwon, and A. H. Zewail, Science **325**, 181 (2009).

[59] V. V. Baranov and V. V. Kabanov, Phys. Rev. B **89**, 125102 (2014).